Nuclear Engineering and Technology 53 (2021) 2582–2590

Contents lists available at ScienceDirect

Nuclear Engineering and Technology

journal homepage: www.elsevier.com/locate/net

Original Article

Effect of mechanical alloying on the microstructural evolution of a ferritic ODS steel with (Y–Ti–Al–Zr) addition processed by Spark Plasma Sintering (SPS)

E. Macía [a, *], A. García-Junceda [b], M. Serrano [c], S.J. Hong [d], M. Campos [a, **]

[a] Dpt. Materials Science and Engineering, IAAB, Universidad Carlos III de Madrid (UC3M), Av. de La Universidad 30, 28911, Leganés, Spain
[b] IMDEA Materials Institute, C/ Eric Kandel 2, 28906, Getafe, Spain
[c] Structural Materials Division, Technology Department, CIEMAT, Avda de La Complutense 22, 28040, Madrid, Spain
[d] Division of Advanced Material Engineering Kongju National Univerity, South Korea

ARTICLE INFO

Article history:
Received 14 August 2020
Received in revised form
30 January 2021
Accepted 1 February 2021
Available online 10 February 2021

Keywords:
ODS steel
Mechanical alloying
Spark plasma sintering (SPS)
Recrystallization
Small punch test

ABSTRACT

The high-energy milling is one of the most extended techniques to produce Oxide dispersion strengthened (ODS) powder steels for nuclear applications. The consequences of the high energy mill process on the final powders can be measured by means of deformation level, size, morphology and alloying degree. In this work, an ODS ferritic steel, ***Fe–14Cr–5Al–3W-0.4Ti-0.25Y_2O_3-0.6Zr***, was fabricated using two different mechanical alloying (MA) conditions (***M_{std}*** and ***M_{act}***) and subsequently consolidated by Spark Plasma Sintering (SPS). Milling conditions were set to evidence the effectivity of milling by changing the revolutions per minute (rpm) and dwell milling time. Differences on the particle size distribution as well as on the stored plastic deformation were observed, determining the consolidation ability of the material and the achieved microstructure. Since recrystallization depends on the plastic deformation degree, the composition of each particle and the promoted oxide dispersion, a dual grain size distribution was attained after SPS consolidation. M_{act} showed the highest areas of ultrafine regions when the material is consolidated at 1100 °C. Microhardness and small punch tests were used to evaluate the material under room temperature and up to 500 °C. The produced materials have attained remarkable mechanical properties under high temperature conditions.

1. Introduction

Along the last decades, the ferritic ODS steels have been postulated as one of the most important candidates structural material for the new nuclear energy applications (GenIV and fusion reactors). Its interest lies on the good mechanical properties under high temperature conditions resulting from the combination of a high density thermally stable oxides dispersed into the ferritic matrix and the effect of the dual grain size distribution [1–3].

Promoting the ODS mechanism relies on the generation of a fine and dense amount of nano-oxides. These nano-precipitates block the motion of dislocations improving the behaviour under high temperatures [4,5]. Traditionally, Y_2O_3 additions were the most suitable way to facilitate the nano-oxides precipitation. However, refining the size of the different precipitates is mandatory to increase the mechanical properties. With this aim, Ti was added refining the Y_2O_3 precipitates by forming the non-stoichiometric Y–Ti–O nanoclusters whose nature and size increase the performance of the ODS steel. S. Ukai et al. were the first to notice this behaviour [6–8]. Furthermore, in ODS steels, the Al addition of around 5%, replaces Ti as a former of Ti–Y–O nanoclusters favouring the precipitation of Y–Al–O oxides that may be too big to improve the behaviour at high temperatures. In this sense, Zr is added to produce Y–Zr–O nano-oxides, refining the oxide precipitates sizes and increasing the thermal stability [9–13]. Among others, Dou et al. [10] studied that the presence of Zr could lead to a refinement of the nano-oxides in the metal matrix of Al containing ODS steels, which leads to an increase in the high temperature behaviour meanwhile the corrosion resistance is not modified [13–16].

* Corresponding author.
** Corresponding author.
E-mail addresses: eric.macia@uc3m.es (E. Macía), andreajunceda@gmail.com (A. García-Junceda), marta.serrano@ciemat.es (M. Serrano), hongsj@kongju.ac.kr (S.J. Hong), monica.campos@uc3m.es (M. Campos).

https://doi.org/10.1016/j.net.2021.02.002

In fact, the MA step is used to incorporate the fine oxides particles into the material. Usually, prealloyed powders (in this research Fe–Cr–W–Al) are handled to favour the right dispersion of the different alloying elements and the oxides precursors [17]. Consequently, Y_2O_3 is introduced directly as an oxide to be dissolved by high energy milling and recombined during consolidation with the different oxide precursors (Ti, Zr and Al) to precipitate as a complex nano oxide [17–21] forming the different species of precipitates reported on the literature [10,12,22–25]. Along with, high energy milling results in a severe deformation, welding and fragmentation leading into a highly deformed powder.

Traditionally, ODS steels were consolidated by Hot isostatic pressing (HIP) or Hot extrusion (HE) [26,27]. However, the use of Field assisted sintering techniques (FAST) such as Spark plasma sintering (SPS) can be considered if the material needs to be fully densified [28–32]. The powder is placed in a graphite die where is simultaneously uniaxially pressed and heated by Joule effect provided by pulses of high intensity current. This method allows fast heating rates and thus, short densification cycles (less than 15 min). Hence the recrystallization of the nanostructure obtained during the milling step is inhibited. Temperature, pressure, holding time, heating rate could have a dramatic effect on the final microstructure and densification [33,34].

Understanding how the microstructure is determined by the mechanical alloying parameters is one of the main objectives of this research. Besides, the mechanical properties were studied in order to analyse the effect of Zr addition, by comparing processed materials of this research with alloys previously obtained where the prealloyed powder was MA with 0.4 Ti and 0.25 Y_2O_3 –wt.%-(14AlODSTi) [35]. Finally, the material is evaluated under high temperature conditions by comparing small punch samples with the ones provided by GETMAT project material (reference steel processed by MA and HE at 1100 °C and finally annealed for 1.5 h at 1050 °C) [36,37].

This research represents the starting point of the work developed in Ref. [38] focused on the SPS consolidation effects. In this study, there were an extensive analysis of how the effect of the heating rate consolidation during SPS could determine the grain growth. However, this paper represents a previous step which discusses the influence that the MA has on the microstructure and on the properties of the material.

2. Experimental procedure

The ferritic ODS steels with the composition displayed in Table 1 were manufactured by using MA and SPS. The starting raw materials were a gas atomized prealloyed powder Fe–14Cr–5Al–3W (wt.%) provided by Sandvik Osprey, a pure elemental Ti powder from Gfe mbH, a Y_2O_3 nanopowder from TJ Technologies & Materials Inc., and a pure elemental Zr powder from Good Fellow.

The MA processes were performed in a horizontal attritor (ZOZ CM01), under a constant flow of highly pure Ar atmosphere (99.9995 vol%) with previous vacuum purges to control the quality of the milled atmosphere. The ball to powder ratio was 20:1. The processes followed are shown in Fig. 1. Two different milling cycles were used and named as standard milling (M_{std}) and activated milling (M_{act}). The final purpose is to optimize the involved milling energy, which is defined by collisions efficiency, i.e., by the rotational speed (rpm) and the overheating generated during the collisions when grinding media remains constant. Normally, to control the heat released in collisions, millings cycles contains dwells of a certain time at the highest rpm, followed by some slow motions intervals, to cool down the powders and prevent the welding with balls and vessel. In this case, the involved energy is nominally higher for the M_{act} cycle. Therefore, M_{act} parameters increase the dwell time at slow rpm.

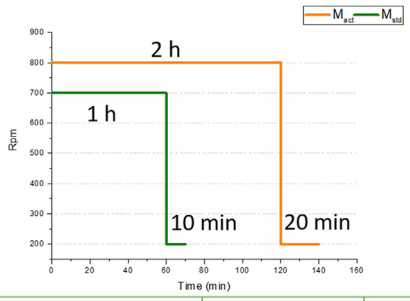

Parameters	M_{Std}	M_{act}
Milling rate	700 rpm	800 rpm
Milling atmosphere	Constant flow of Argon	
Milling temperature	Room temperatura (25-30 °C)	
Milling routine	Continues milling	
Effective milling time	60 h	50 h
Resting time	10 min	20 min

Fig. 1. Mechanical alloying standard (M_{std}) and Mechanical alloying activated (M_{act}) parameters.

The powder blending was slightly different for both processes. Before applying the M_{act} conditions, 14ZrODS powder was mechanically blended for 2 h at 200 rpm inside the attritor mill. However, before the MA step using M_{std} parameters, a Turbula equipment (Turbula shaker mixer WAB) mixed 14ZrODS powders.

Once powders are characterized by X-Ray diffraction, the Scherrer method was selected to analyse the evolution of the crystallite size (L) and microstrain (ε) values with milling time, considering the most intense peak of the milled powders. The diffraction patterns were collected on a X'pert Phillips using Cu-Kα radiation, with a step size of 0.02° and 7.6 s per step.

To determine the powder shape, size and final distribution, a scanning electron microscope (SEM) (Philips XL-30) and a laser particle size analyser (Mastersizer 2000) were used. Finally, to determine the carbon and oxygen contamination LECO CS-200 and LECO TC-500 were respectively used.

To consolidate MA powder, SPS Sintex Inc. model 3.20 MK-V was used. Within this aim, the powder was placed in a graphite die of 20 mm diameter and 5 mm thickness and heated by Joule effect provided by pulses of high intensity current to the selected temperature using a heating rate of 100 °C/min with a dwell of 3 min, under 50 MPa pressure, from R.T. The process was performed under low vacuum (10^{-2}-10^{-3} mbar) to avoid oxygen enrichment. Besides, a suspension of Boron Nitride (BN) was sprayed on the graphite die walls to protect the powder from the carbon.

To analyse the effect on the final densification of the material or tailoring the grain size distribution, the selected temperature was 1100 °C (Table 2). The temperature was controlled by using two

Table 1
Composition (wt.%) of the processed ferritic ODS (powder label: P: Prealloyed, E: elemental).

	Fe	Cr	Al	W	Ti	Zr	Y_2O_3
14ZrODS	Balance^P				0.4^E	0.6^E	0.25

Table 2
SPS cycles performed on 14ZrODS powders.

Cycle	Sample Label
100 °C/min, 1100 °C,50 MPa, 3 min	***M_{std}, 1100; M_{act}, 1100***

thermocouples in the upper punch and in the centre of the die wall. The density of the sintered discs was measured by image analysis handling JMicroVision free software.

In order to study the microstructure of the consolidated discs, samples were conventionally grounded and polished up to alumina of 0.03 μm and finished by OPS suspension of 0.01 μm. After this, electropolishing was applied (Struers, Tecnupol) to enhance the quality of the surface.

The microstructure was evaluated by SEM (Philips XL-30 and FEI Teneo) and Field emission gun-focus ion beam (FEG-FIB) microscopy coupled to energy dispersive x-ray (EDX) and electron backscatter diffraction (EBSD) detectors (Zeiss Crossbeam 1540 focused ion beam). EBSD patterns of transversal section with respect to the compression direction were performed using a step size of 80 nm with a tolerance angle of 2° to determine the grain size distribution.

To evaluate the mechanical properties at R.T., Vickers microhardness (Zwick Roell) was measured applying 200 g during 10 s, where each value corresponds to the average of 20 indentations considering the complete bimodal microstructure.

To analyse the properties achieved at different temperatures, covering from R.T. to 500 °C, small punch test was performed on discs prepared from the transversal section to the press direction of SPS, at a displacement rate of 0.3 mm/min. The specimens (3 mm diameter and 0,250 mm thickness) were finished as mirror-like surfaces to evaluate the fracture mode and ductility.

3. Results

3.1. Characterization, as-milled powder

Both 14ZrODS M_{std} and M_{act} powders presented, after 60 and 50 h respectively, an irregular morphology composed by smaller particles in which M_{std} showed a particle size (D_{50}) of 46 μm meanwhile M_{act} produced a 77 μm particle size (Fig. 2).

During MA, the process of plastic deformation produces repeated fracturing and cold welding on particles that determines the progression of the alloying. During the first milling steps, particles start to adopt a flake-like shape and from that point, cold welding will be the dominant mechanism. As the milling process continues, the powder is hardened and consequently fracture step starts, leading into a reduction of the mean particle size. Further collisions promote welding between particles as well [18].

The minimum crystallite value after 60 h (M_{std}) and 50 h (M_{act}) of milling is close to that studied for pure Fe in Ref. [39]. To obtain a nanostructured powder, it is necessary to ensure a high microstrain level and low crystallite size as milling time progresses, as reported in Refs. [32,38]. Once a critical level of microstrain is reached, the crystallite size remains stable, attaining a steady state with milling time, as shown in Fig. 3 [40,41].

Table 3 compares the final characteristics of milled powders including the initial features of the prealloyed grade. Both milling parameters achieved similar crystallographic parameters even if the attained particles size is different between both powders (46 vs 77 μm). Surprisingly, M_{act} presented powders with higher dislocation strengthening which is directly related to dislocation density through equation (1) and to the strengthening promoted through equation (2) [38,42]:

$$\rho = 14.4\frac{\varepsilon^2}{b^2} \quad (1)$$

$$\sigma_{dis} = M\alpha_d Gb\sqrt{\rho} \quad (2)$$

where ε represents the achieved microstrain, M is the Taylor factor (3.06), G is the shear modulus of iron (85 GPa), b is the burger vector (0.252 nm assumed Fe pure lattice), α is a constant (1/3) and ρ is the dislocation density as it is reported in Ref. [38].

In this case, the enhancement attained with M_{act} milling mode is clear. At the end of MA, the plastic deformation stored, and the alloying degree attained are different between each particle.

The interstitial levels showed on Table 4 remarks the good powder quality.

3.2. Characterization of consolidated samples: effect of the milling parameters on the final sample

In order to analyse the effect of the milling parameters (M_{std} vs M_{act}) on the final densification and final microstructure, the cross section of the samples was evaluated studying the reached densities (Fig. 4).

The density is slightly influenced by the milling parameters (see Table 5). Initial differences on the particle size (46 μm vs 77 μm) could determine different distributions of temperatures during the consolidation. Smaller particle size provides better temperature homogenization, leading into a higher consolidation at lower temperatures (1100 °C). The mass transport phenomenon, responsible of the growth on the sintering necks is favoured by smaller particles, as previously reported by S.Diouf et al. [43].

Nonetheless, regardless of the selected milling cycle, accurate values of densities are achieved, for all samples (Table 5). This should lead into reproducible mechanical properties.

SPS consolidation may reduce the grain growth of the material comparing to other sintering techniques, nevertheless it could not avoid the recrystallization [44]. The thermal activation leads to crystallite growth meanwhile the internal strain decreases. Consequently, the final values attained are similar to the ones presented on the prealloyed powder as stated on Fig. 5.

These sintered ODS steels evolve into a dual grain size microstructure (Fig. 6) providing a material with a better balance

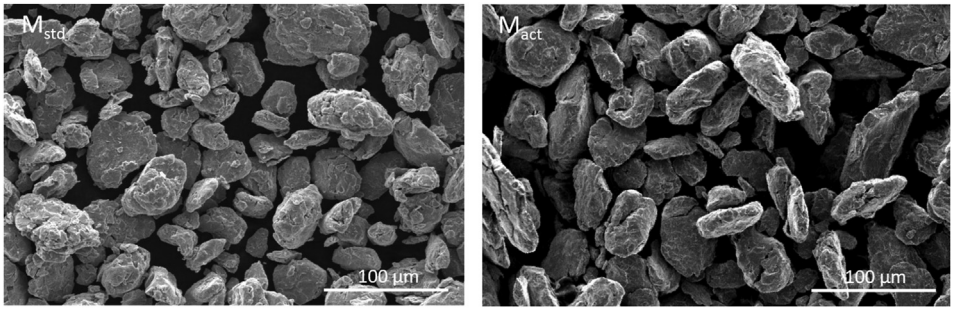

Fig. 2. 14ZrODS powders details after 60 h of MA (left side) and 50 h (right side).

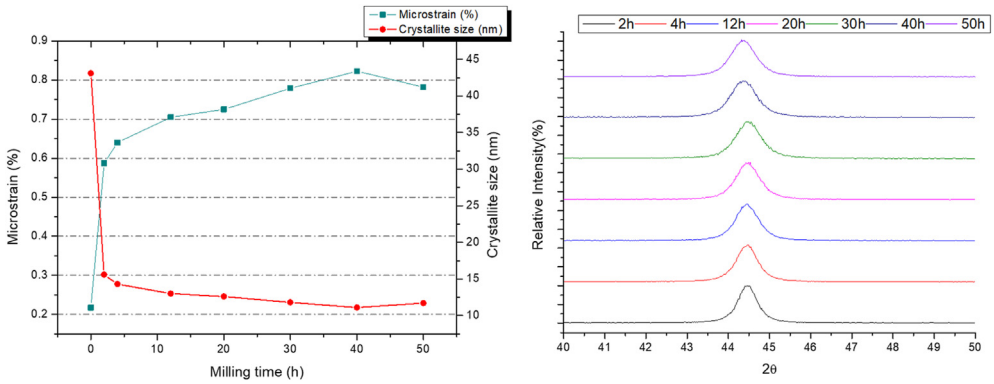

Fig. 3. M_{act} 14ZrODS powders:Microstrain and crystallite size evolution during the milling time calculated by using Scherrer method on the most intense peak (110).

Table 3
Particle size distribution and crystallographic parameters of the MA powders under M_{std} and M_{act} conditions.

	D_{10} (μm)	D_{50} (μm)	D_{90} (μm)	L (nm)	ε (%)	ρ_{dis} (m^{-2})	σ_{dis} (MPa)
Preal.14Al	12	30	62	43.1	0.217	$1.07 \cdot 10^{15}$	781
14ZrODS (M_{std})	22	46	92	12.1	0.762	$1.32 \cdot 10^{16}$	2505
14ZrODS (M_{act})	40	77	151	11.7	0.782	$1.39 \cdot 10^{16}$	2570

Table 4
Carbon and oxygen analysis of M_{std} and M_{act} conditions.

	%C	%O
14ZrODS (M_{std})	0.195	0.010
14ZrODS (M_{act})	0.149	0.110

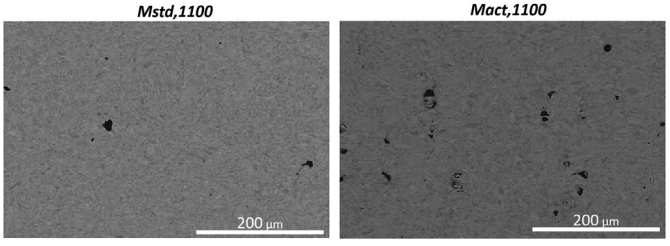

Fig. 4. Consolidation evolution with the different milling parameters.

Table 5
Samples densities using different milling parameters (%).

Nomenclature	M_{std},1100	M_{act}, 1100
Density (%)	99.8 ± 0.2	98.7 ± 0.5

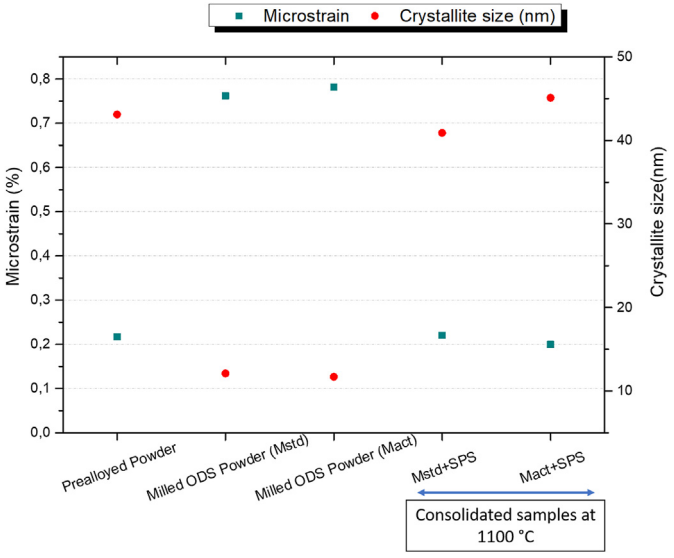

Fig. 5. Microstrain (%) and crystallite size (nm) values in prealloyed powders, milled powders and after SPS consolidation samples.

between toughness/strength resulting in a high-performance material at room and high temperature. During the sintering process, each particle recovers and recrystallizes following different stages leading to an inhomogeneous recrystallization.

Even if the use BN layer during SPS tries to prevent the carbon diffusion from the graphite die, some carbides (from 1 to 5 μm) are decorating the grain boundaries and also formed inside of grains (see Fig. 6). As Garcia et al. reported [35], these carbides with MC and M_6C stoichiometry, contain Cr and Cr–W and they are frequently located in ODS alloys coming from MA powders, regardless of the method used for consolidating the material (HIP, SPS or HE) as it was also stated in Refs. [28,45].

On first instance, it seems that M_{std} provides a microstructure mainly composed by micrometrics grains (micrograins) with some ultrafine regions (UF), which represent less than 3% of the whole microstructure (Fig. 7, left side). On the contrary, M_{act} provides a marked dual grain size microstructure, where almost 10% of the entire microstructure are ultrafine regions (Fig. 7 right side).

It is important to highlight that not only the area covered by the UF is bigger but also, the grain size inside this area is smaller (Fig. 7, ultrafine grains).

The EBDS inverse pole figures maps (IPF Y) show the different crystal orientation provided by the mechanical alloying process, where the absence of texture has been also reported as typical of this alloy consolidated by SPS [22,38].

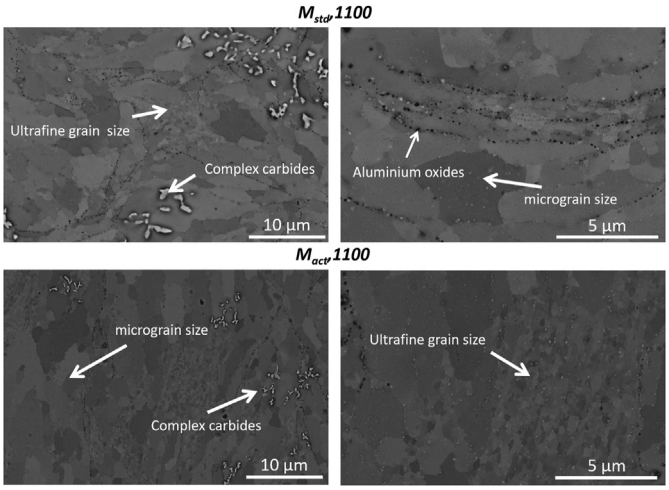

Fig. 6. Analysed microstructure on M_{std} and M_{act} powders after being consolidated at 1100 °C by using SPS.

3.3. Evaluation of mechanical properties

Since the selected composition is the same for all the processed materials, mechanical alloying step would have a direct effect on the mechanical response. This relationship is studied by means of microhardness and SP tests.

3.3.1. Room temperature evaluation

Regardless of the milling conditions, all the consolidated ODS steels presented a good microhardness level, thanks to the proper densification and to the oxide dispersion strengthening mechanism (see Fig. 8) [26,30,46].

Zr addition seems to improve the microhardness with respect to 14Al-ODS-Ti. However, the best value was the one obtained for M_{act} conditions consolidated at 1100 °C.

By using the relationship between hardness and strength, to get an approximate value of Yield Strength where HV ~3 σ (transferring HV units to MPa) [47], it is possible to connect these results with the UF area developed on each 14ZrODS steel (Table 6). The enhancement on density and the presence of Zr contribute to the performance improvement.

3.3.2. High temperature evaluation

The SP test results are shown through the load deflection curves (Fig. 9). As it was stated in Ref. [38], the bimodal microstructure of 14ZrODS together with the oxides pinning effect (conditioned by Zr addition) are responsible of the different behaviour when they are compared with other Zr free ferritic ODS as 14AlODS-Ti.

Both milling conditions (M_{act} and M_{std}) enhance higher performance at RT and 500 °C compare to Zr free ODS (14Al-ODS-Ti). Even if at room temperature GETMAT steel is far better than 14ZrODS steels (Fig. 9, top left side), when test temperature rises to 300 °C and 500 °C, the maximum load and deflection achieved are totally comparable. The refinement of the microstructure reached by using FAST consolidation techniques and by the Zr addition are increasing the behaviour under high temperature.

Nevertheless, at high temperature, the grain refinement of steels processed by M_{act} conditions provides a minimal effect on the final properties attained; contrary of what it was expected from the results obtained by micro hardness test (Fig. 9, bottom). This behaviour is related to the higher contribution of the nano-oxides precipitates to the final strengthening of the material under high temperature conditions as it is reported in [38,48,49].

Fractured specimens (Fig. 10) were divided into two groups according to cracks morphology; rounded for ductile materials, star shape for brittle materials. The cracks shape is opened and

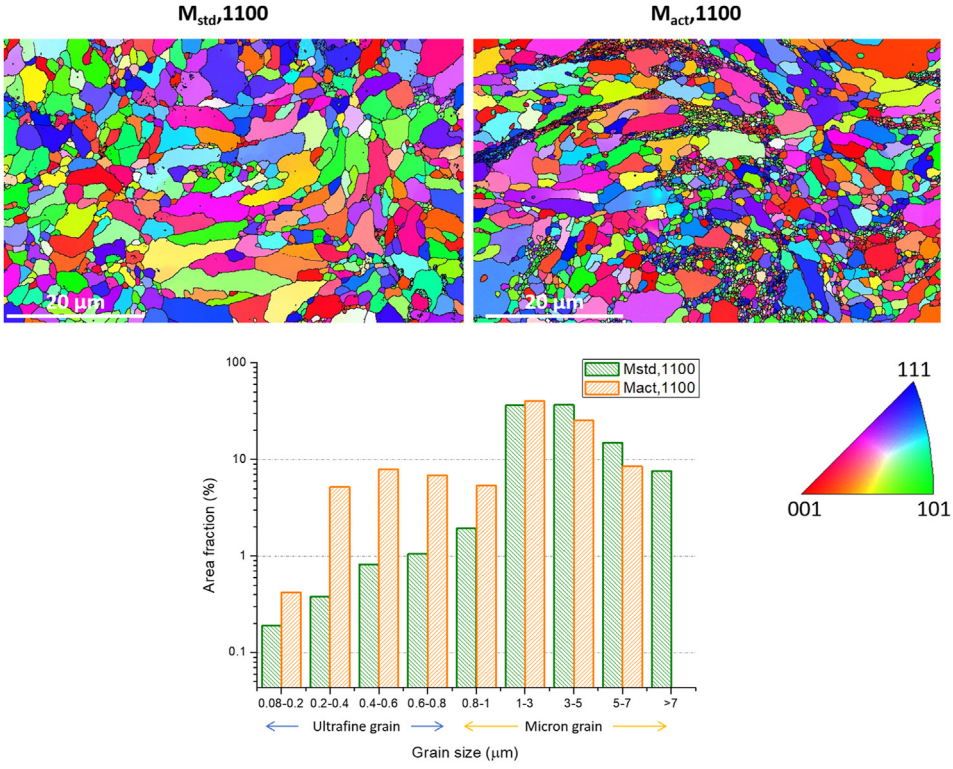

Fig. 7. Analysed bimodal microstructure on M_{std} and M_{act} consolidated samples by using EBSD analysis.

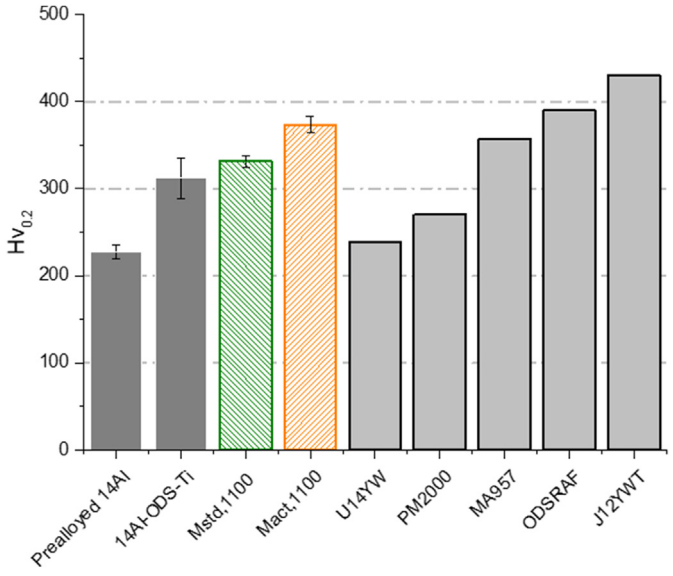

Fig. 8. ODS steels comparative microhardness [33].

Table 6
14ZrODS yield strength calculated through microhardness measurements, regarding to milling cycle and percentage of the area covered with UF grains.

Nomenclature	M_{std}, 1100	M_{act}, 1100
σ_y (MPa)	1081	1219
%UF Area	2	20

circumferentially oriented, corresponding to the fracture mode for ductile-brittle samples [37,50]. The Zr addition and the grain size distribution support the ductility of the material.

Independently on the developed microstructure, both materials presented similar fracture behaviour independently of the attained ultrafine regions.

4. Discussion

The bimodal grain size microstructure is characteristic of ODS ferritic steels [30] processed by MA, independently of using HIP or SPS as it is reported by I. Hilger et al. in Ref. [51]. Generally, the final microstructure for 14ZrODS steels is determined by two parameters which are controlling the grain growth. First, after mechanical alloying process, the oxide formers elements are ready to combine with oxygen and to precipitate in small nanoclusters and nano-oxides during consolidation. Both produce a strong pinning effect blocking the grain growth. Second, during MA, particles are unequally deformed determining the heterogeneous stored energy and the ability of recrystallization [17,29,51–54]. In this case, M_{std} and M_{act} milling conditions have developed ODS steels whose microstructures are sensibly different. M_{act} parameters favour microstructures composed by UF grain areas (around 10%), meanwhile M_{std} conditions promote a microstructure composed especially by micrometric grains (less than 3% is covered by UF regions).

Thanks to an in situ X-ray diffraction experiment N. Sallez et al. [44] observed that nanoclusters precipitate on the alloy around 800 °C, therefore from this point, the grain growth is highly determined by this nano-precipitation. As the M_{std} and M_{act} conditions have the same raw material composition (see experimental procedure) and even if the nano-oxide behaviour is not quantified, equivalent nanoclusters nature, density and size could be developed. Besides, other parameters are controlling the grain growth evolution during SPS to explain the differences between both ferritic steels.

The amount of plastic deformation stored on each particle after the MA can also contribute to the final microstructure [31]. The measured dislocation density for both milled powders is similar (around 10^{16} m^{-2}, see Table 3) and the first recovery by dislocation

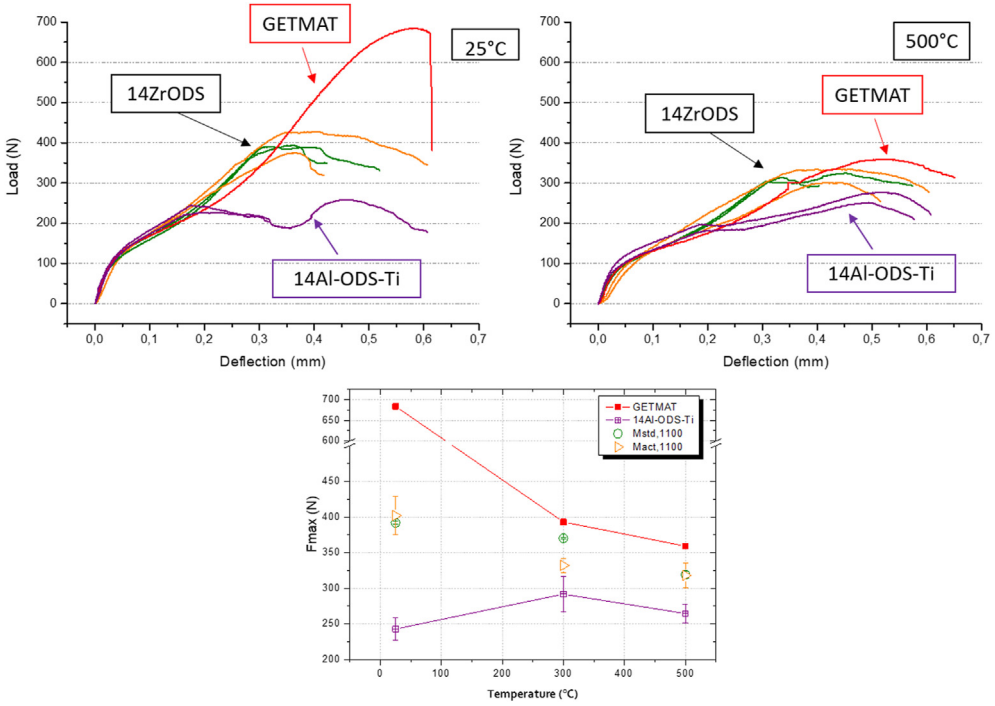

Fig. 9. Small punch tests at different temperatures (Rt.left side and 500 °C right side) and F_{max} at different temperatures.

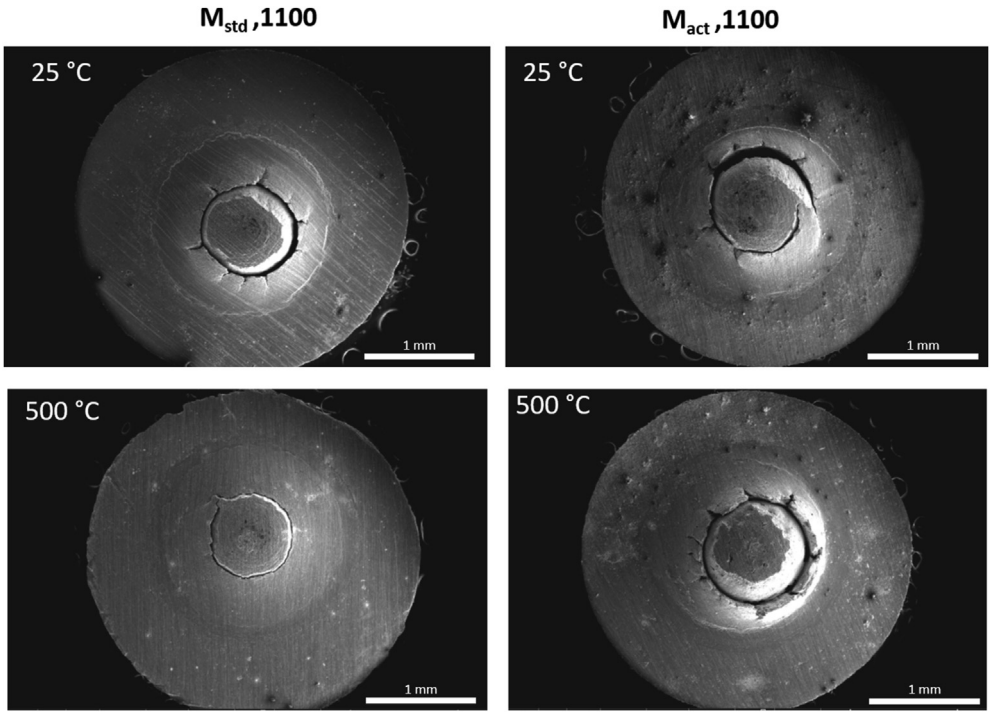

Fig. 10. Small punch fracture specimens for different milling conditions and tested temperatures.

rearrangement will be only affected by the particle size distribution. In this step crystallite size would be increased. As SPS temperature rises grain growth and precipitation of nano oxides appears. Both phenomena will compete and lead to the bimodal grain size distribution; on one hand, recrystallization induces a fast grain growth, on the other side, pinning effect of nano precipitates stops the evolution. The uneven deformation and alloying degree on each milled particle make the evolution of the grain size distribution different between all of them. That means that recrystallization phenomena take places at different temperatures depending on deformed particles (see Fig. 11). Particles highly deformed will have a lower recrystallization temperature.

An inhomogeneous and competitive grain growth appears on the material during consolidation. And hence, new nuclei are formed at expenses to growth to the unrecovered ones, consequently recrystallized grains will growth at expenses of the brand-

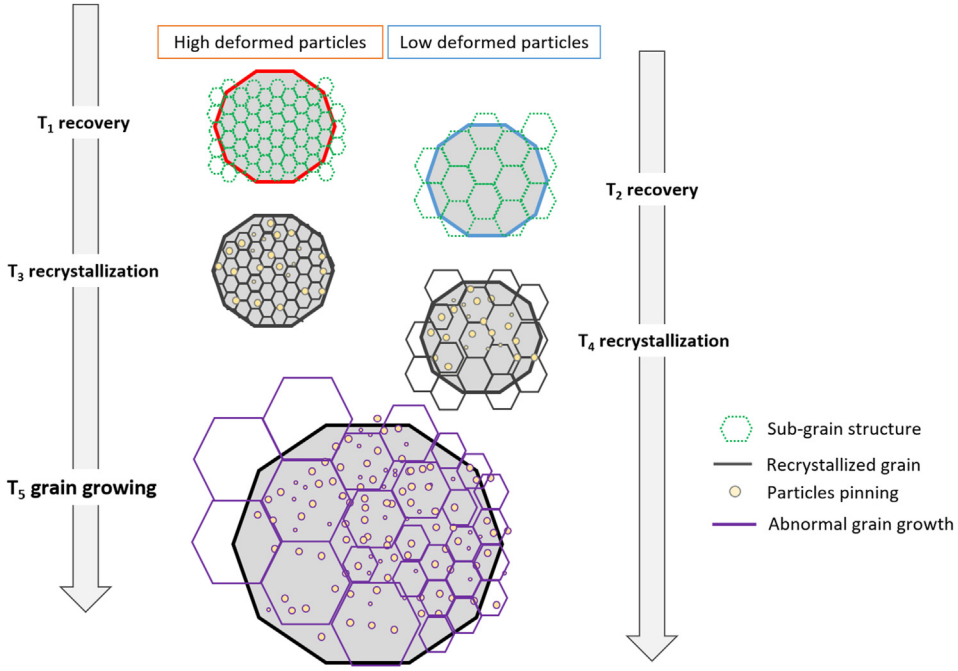

Fig. 11. Schematic recovery, recrystallization and abnormal grain growth taking place in ODS steels.

new deformed ones low deformed ones [30,48]. This phenomenon leads into bimodal grain size microstructure as it is schematized in Fig. 11.

The influence of the particle size distribution for each milling conditions and mean particle size should be also considered. During consolidation, the distribution of temperature will be more homogeneous as the particle size is narrower and the mean particle size is smaller, hence the recrystallization will progress uniformly, as that is the case of the ferritic ODS processed with M_{std} cycle (see Table 3) where the amount of UF grains are close to 3%. Besides, surface amount for the same volume of powder will be higher for this condition and recrystallization will be enhanced.

Both I. Higler et al. in Ref. [17] and X. Boulnat et al. in Ref. [29] reported a similar grain size distribution to the one studied here. In their case, they observed how uniform deformed particles lead to narrower bimodal microstructure.

The stability of the precipitates influenced by the addition of Zr influence the mechanical properties [29] since the ODS steels processed by both MA conditions have reached good mechanical properties at room temperature and remarkable properties under high temperature. Precipitation as stated by N. Sallez et al. [44] is not only influencing the abnormal grain growth, it is also the principal responsible of the stability of the microstructure as soon as it is developed. This should explain the outstanding behaviour attained under high temperature conditions in the small punch tests [29,51].

5. Conclusions

In this research, a prealloyed powder (Fe−14Cr−3W−5Al) has been mechanically alloyed with Y_2O_3, Ti and Zr (14ZrODS) by using two different parameters of MA (M_{std} and M_{act}) and then consolidated by SPS to improve the efficiency on the ODS ferritic steels production. The main conclusions are:

- High-energy milling cycles have introduced a massive amount of plastic deformation, with dislocation density of 10^{16} m^{-2} and oxide promoters distributed all over the particles.
- Different milling parameters provided different microstructure and different consolidation when a SPS sintering at 1100 °C is performed. Probably, the way in which the particles are deformed during the process promotes this behaviour.
- M_{act} milling parameters (800 rpm, 50 h) favour the dual size microstructure on the sample, leading to better mechanical response at room temperature. However, since Zr addition is conditioned the pinning effect, the response at high temperature evaluated by SP is similar for both steels and comparable to GETMAT material.

Declaration of competing interest

The authors declare that they have no known competing financial interests or personal relationships that could have appeared to influence the work reported in this paper.

Acknowledgments

Authors want to acknowledge Ferro-Ness project and Ferro-Genesys project funded by MINECO under National I + D + I program MAT2016-80875-C3-3-R and MAT2013-47460-C5-5-P. The authors gratefully acknowledge the help received from Daniel Plaza Lopez during the Small-Punch tests.

References

[1] S. Ukai, M. Fujiwara, Perspective of ODS alloys application in nuclear environments, J. Nucl. Mater. 307–311 (2002) 749–757, https://doi.org/10.1016/S0022-3115(02)01043-7.
[2] N. Cunningham, Y. Wu, D. Klingensmith, G.R. Odette, On the remarkable thermal stability of nanostructured ferritic alloys, Mater. Sci. Eng. 613 (2014) 296–305, https://doi.org/10.1016/j.msea.2014.06.097.
[3] M.K. Miller, D.T. Hoelzer, E.a. Kenik, K.F. Russell, Stability of ferritic MA/ODS alloys at high temperatures, Intermetallics 13 (2005) 387–392, https://doi.org/10.1016/j.intermet.2004.07.036.
[4] K. Rajan, V.S. Sarma, T.R.G. Kutty, B.S. Murty, Hot hardness behaviour of ultrafine grained ferritic oxide dispersion strengthened alloys prepared by mechanical alloying and spark plasma sintering, Mater. Sci. Eng. 558 (2012) 492–496, https://doi.org/10.1016/j.msea.2012.08.033.
[5] C.-L. Chen, A. Richter, R. Kögler, G. Talut, Dual beam irradiation of nanostructured FeCrAl oxide dispersion strengthened steel, J. Nucl. Mater. 412 (2011) 350–358, https://doi.org/10.1016/j.jnucmat.2011.03.041.
[6] S. Ohtsuka, S. Ukai, M. Fujiwara, T. Kaito, T. Narita, Improvement of 9Cr-ODS martensitic steel properties by controlling excess oxygen and titanium contents, J. Nucl. Mater. 329–333 (2004) 372–376, https://doi.org/10.1016/j.jnucmat.2004.04.043.
[7] S. Ukai, S. Mizuta, M. Fujiwara, T. Okuda, T. Kobayashi, Development of 9cr-ods martensitic steel claddings for fuel pins by means of ferrite to austenite phase transformation, J. Nucl. Sci. Technol. 39 (2002) 778–788, https://doi.org/10.1080/18811248.2002.9715260.
[8] S. Ohtsuka, S. Ukai, M. Fujiwara, T. Kaito, T. Narita, Nano-structure control in ODS martensitic steels by means of selecting titanium and oxygen contents, J. Phys. Chem. Solid. 66 (2005) 571–575, https://doi.org/10.1016/j.jpcs.2004.06.033.
[9] A. Kimura, R. Kasada, N. Iwata, H. Kishimoto, C.H. Zhang, J. Isselin, P. Dou, J.H. Lee, N. Muthukumar, T. Okuda, M. Inoue, S. Ukai, S. Ohnuki, T. Fujisawa, T.F. Abe, Development of Al added high-Cr ODS steels for fuel cladding of next generation nuclear systems, J. Nucl. Mater. 417 (2011) 176–179, https://doi.org/10.1016/j.jnucmat.2010.12.300.
[10] P. Dou, A. Kimura, R. Kasada, T. Okuda, M. Inoue, S. Ukai, S. Ohnuki, T. Fujisawa, F. Abe, TEM and HRTEM study of oxide particles in an Al-alloyed high-Cr oxide dispersion strengthened steel with Zr addition, J. Nucl. Mater. 444 (2014) 441–453, https://doi.org/10.1016/j.jnucmat.2013.10.028.
[11] R. Gao, T. Zhang, X.P. Wang, Q.F. Fang, C.S. Liu, Effect of zirconium addition on the microstructure and mechanical properties of ODS ferritic steels containing aluminum, J. Nucl. Mater. 444 (2014) 462–468, https://doi.org/10.1016/j.jnucmat.2013.10.038.
[12] J. Isselin, R. Kasada, A. Kimura, T. Okuda, M. Inoue, S. Ukai, S. Ohnuki, T. Fujisawa, F. Abe, Effects of Zr addition on the microstructure of 14%Cr4%Al ODS ferritic steels, Mater. Trans. 51 (2010) 1011–1015, https://doi.org/10.2320/matertrans.MBW200923.
[13] A. García-Junceda, N. García-Rodríguez, M. Campos, M. Cartón-Cordero, J.M. Torralba, Effect of zirconium on the microstructure and mechanical properties of an Al-alloyed ODS steel consolidated by FAHP, J. Am. Ceram. Soc. 98 (2015) 3582–3587, https://doi.org/10.1111/jace.13691.
[14] W. Li, T. Hao, R. Gao, X. Wang, T. Zhang, Q. Fang, C. Liu, The effect of Zr, Ti addition on the particle size and microstructure evolution of yttria nanoparticle in ODS steel, Powder Technol. 319 (2017) 172–182, https://doi.org/10.1016/J.POWTEC.2017.06.041.
[15] H. Zhang, C. Zhang, Y. Yang, Y. Meng, J. Jang, A. Kimura, Irradiation hardening of ODS ferritic steels under helium implantation and heavy-ion irradiation, J. Nucl. Mater. 455 (2014) 349–353, https://doi.org/10.1016/j.jnucmat.2014.06.062.
[16] H. Xu, Z. Lu, D. Wanga, C. Liu, Effect of zirconium addition on the microstructure and mechanical properties of 15Cr-ODS ferritic Steels consolidated by hot isostatic pressing, Fusion Eng. Des. 114 (2017) 33–39, https://doi.org/10.1016/J.FUSENGDES.2016.11.011.
[17] I. Hilger, F. Bergner, T. Weißgärber, Bimodal grain size distribution of nanostructured ferritic ODS Fe − Cr alloys, J. Am. Ceram. Soc. 3581 (2015) 3576–3581, https://doi.org/10.1111/jace.13833.
[18] J.M. Torralba, L. Fuentes-Pacheco, N. García-Rodríguez, M. Campos, Development of high performance powder metallurgy steels by high-energy milling, Adv. Powder Technol. 24 (2013) 813–817, https://doi.org/10.1016/j.apt.2012.11.015.
[19] M. Nagini, R. Vijay, M. Ramakrishna, a.V. Reddy, G. Sundararajan, Influence of the duration of high energy ball milling on the microstructure and mechanical properties of a 9Cr oxide dispersion strengthened ferritic–martensitic steel, Mater. Sci. Eng. 620 (2015) 490–499, https://doi.org/10.1016/j.msea.2014.10.050.
[20] R. Xie, Z. Lu, C. Lu, C. Liu, Effects of mechanical alloying time on microstructure and properties of 9Cr–ODS steels, J. Nucl. Mater. 455 (2014) 554–560, https://doi.org/10.1016/J.JNUCMAT.2014.08.042.
[21] M.J. Alinger, G.R. Odette, D.T. Hoelzer, On the role of alloy composition and processing parameters in nanocluster, Fusion Mater. Semiannu. Prog. Rep. (2008) 53–78.
[22] A.G. Junceda, E. Macía, D. Garbiec, M. Serrano, J.M. Torralba, Effect of Small Variations in Zr Content on the Microstructure and Properties of Ferritic ODS Steels Consolidated by SPS, 2020, https://doi.org/10.3390/met10030348.

[23] J. Ren, L. Yu, Y. Liu, C. Liu, H. Li, J. Wu, Effects of Zr addition on strengthening mechanisms of Al-alloyed high-Cr ODS steels, Materials 11 (2018) 1–13, https://doi.org/10.3390/ma11010118.
[24] W.Z. Xu, L.L. Li, M. Saber, C.C. Koch, Y.T. Zhu, R.O. Scattergood, Nano ZrO2 particles in nanocrystalline Fe–14Cr–1.5Zr alloy powders, J. Nucl. Mater. 452 (2014) 434–439, https://doi.org/10.1016/j.jnucmat.2014.05.067.
[25] L. Zhang, L. Yu, Y. Liu, C. Liu, H. Li, J. Wu, Influence of Zr addition on the microstructures and mechanical properties of 14Cr ODS steels, Mater. Sci. Eng. 695 (2017) 66–73, https://doi.org/10.1016/J.MSEA.2017.04.020.
[26] Z. Oksiuta, N. Baluc, Effect of mechanical alloying atmosphere on the microstructure and Charpy impact properties of an ODS ferritic steel, J. Nucl. Mater. 386–388 (2009) 426–429, https://doi.org/10.1016/j.jnucmat.2008.12.148.
[27] Z. Oksiuta, P. Hosemann, S.C. Vogel, N. Baluc, Microstructure examination of Fe-14Cr ODS ferritic steels produced through different processing routes, J. Nucl. Mater. 451 (2014) 320–327, https://doi.org/10.1016/j.jnucmat.2014.04.004.
[28] M.A. Auger, V. De Castro, T. Leguey, A. Muñoz, R. Pareja, Microstructure and mechanical behavior of ODS and non-ODS Fe-14Cr model alloys produced by spark plasma sintering, J. Nucl. Mater. 436 (2013) 68–75, https://doi.org/10.1016/j.jnucmat.2013.01.331.
[29] X. Boulnat, M. Perez, D. Fabregue, T. Douillard, M.H. Mathon, Y. De Carlan, Microstructure evolution in nano-reinforced ferritic steel processed by mechanical alloying and spark plasma sintering, Metall. Mater. Trans. A Phys. Metall. Mater. Sci. 45 (2014) 1485–1497, https://doi.org/10.1007/s11661-013-2107-y.
[30] K.N. Allahar, J. Burns, B. Jaques, Y.Q. Wu, I. Charit, J. Cole, D.P. Butt, Ferritic oxide dispersion strengthened alloys by spark plasma sintering, J. Nucl. Mater. 443 (2013) 256–265, https://doi.org/10.1016/j.jnucmat.2013.07.019.
[31] Z. Li, Z. Lu, R. Xie, C. Lu, C. Liu, Effect of spark plasma sintering temperature on microstructure and mechanical properties of 14Cr-ODS ferritic steels, Mater. Sci. Eng. 660 (2016) 52–60, https://doi.org/10.1016/j.msea.2016.02.073.
[32] B.V. Ponraj, A. Dinesh Kumar, S. Kumaran, Rapid synthesis of oxide dispersion strengthened ferritic alloys through Spark plasma sintering, Mater. Today Proc. 27 (2019) 2661–2666, https://doi.org/10.1016/j.matpr.2019.11.094.
[33] I. Bogachev, E. Grigoryev, O.L. Khasanov, E. Olevsky, Fabrication of 13Cr-2Mo ferritic/martensitic oxide-dispersion-strengthened steel components by mechanical alloying and spark-plasma sintering, JOM (J. Occup. Med.) 66 (2014) 1020–1026, https://doi.org/10.1007/s11837-014-0972-5.
[34] X. Boulnat, D. Fabregue, M. Perez, M.H. Mathon, Y. De Carlan, High-temperature tensile properties of nano-oxide dispersion strengthened ferritic steels produced by mechanical alloying and spark plasma sintering, Metall. Mater. Trans. A Phys. Metall. Mater. Sci. 44 (2013) 2461–2465, https://doi.org/10.1007/s11661-013-1719-6.
[35] N. García-Rodríguez, M. Campos, J.M. Torralba, M.H. Berger, Y. Bienvenu, Capability of mechanical alloying and SPS technique to develop nanostructured high Cr, Al alloyed ODS steels, Mater. Sci. Technol. 30 (2014) 1676–1684, https://doi.org/10.1179/1743284714Y.0000000595.
[36] M. Serrano, M. Hernández-Mayoral, A. García-Junceda, Microstructural anisotropy effect on the mechanical properties of a 14Cr ODS steel, J. Nucl. Mater. 428 (2012) 103–109, https://doi.org/10.1016/j.jnucmat.2011.08.016.
[37] M. Serrano, A. García-Junceda, R. Hernández, M.H. Mayoral, On anisotropy of ferritic ODS alloys, Mater. Sci. Technol. 30 (2014) 1664–1668, https://doi.org/10.1179/1743284714Y.0000000552.
[38] E. Macía, A. García-Junceda, M. Serrano, M. Hernández-Mayoral, L.A. Diaz, M. Campos, Effect of the heating rate on the microstructure of a ferritic ODS steel with four oxide formers (Y-Ti-Al-Zr) consolidated by spark plasma sintering (SPS), J. Nucl. Mater. 518 (2019) 190–201, https://doi.org/10.1016/j.jnucmat.2019.02.043.
[39] F.A. Mohamed, Y. Xun, Correlations between the minimum grain size produced by milling and material parameters, Mater. Sci. Eng. 354 (2003) 133–139, https://doi.org/10.1016/S0921-5093(02)00936-X.
[40] H.J. Fecht, Nanoparticle formation by mechanical attrition, Nanostruct. Mater. 6 (1995) 33–42, https://doi.org/10.1016/0965-9773(95)00027-5.
[41] Y.H. Zhao, H.W. Sheng, K. Lu, Microstructure evolution and thermal properties in nanocrystalline Fe during mechanical attrition, Acta Mater. 49 (2001) 365–375, https://doi.org/10.1016/S1359-6454(00)00310-4.
[42] X. Zhou, Y. Liu, L. Yu, Z. Ma, Q. Guo, Y. Huang, H. Li, Microstructure characteristic and mechanical property of transformable 9Cr-ODS steel fabricated by spark plasma sintering, Mater. Des. 132 (2017) 158–169, https://doi.org/10.1016/j.matdes.2017.06.063.
[43] S. Diouf, A. Molinari, Densification mechanisms in spark plasma sintering: effect of particle size and pressure, Powder Technol. 221 (2012) 220–227, https://doi.org/10.1016/j.powtec.2012.01.005.
[44] N. Sallez, X. Boulnat, A. Borbély, J.L. Béchade, D. Fabregue, M. Perez, Y. De Carlan, L. Hennet, C. Mocuta, D. Thiaudiere, Y. Brechet, In situ characterization of microstructural instabilities: recovery , recrystallization and abnormal growth in nanoreinforced steel powder 87 (2015) 377–389, https://doi.org/10.1016/j.actamat.2014.11.051.
[45] M.A. Auger, V. de Castro, T. Leguey, M.A. Monge, A. Muñoz, R. Pareja, Microstructure and tensile properties of oxide dispersion strengthened Fe–14Cr–0.3Y2O3 and Fe–14Cr–2W–0.3Ti–0.3Y2O3, J. Nucl. Mater. 442 (2013) S142–S147, https://doi.org/10.1016/j.jnucmat.2012.11.001.
[46] M.J. Alinger, G.R. Odette, D.T. Hoelzer, On the role of alloy composition and processing parameters in nanocluster formation and dispersion strengthening in nanostuctured ferritic alloys, Acta Mater. 57 (2009) 392–406, https://doi.org/10.1016/j.actamat.2008.09.025.
[47] P. Zhang, S.X. Li, Z.F. Zhang, General relationship between strength and hardness, Mater. Sci. Eng. 529 (2011) 62–73, https://doi.org/10.1016/j.msea.2011.08.061.
[48] A. Chauhan, F. Bergner, A. Etienne, J. Aktaa, Y. De Carlan, C. Heintze, D. Litvinov, M. Hernandez-Mayoral, E. Oñorbe, B. Radiguet, A. Ulbricht, Microstructure characterization and strengthening mechanisms of oxide dispersion strengthened (ODS) Fe-9 % Cr and Fe-14 % Cr extruded bars, J. Nucl. Mater. 495 (2017) 6–19, https://doi.org/10.1016/j.jnucmat.2017.07.060.
[49] M. Dadé, J. Malaplate, J. Garnier, F. De Geuser, F. Barcelo, P. Wident, A. Deschamps, Influence of microstructural parameters on the mechanical properties of oxide dispersion strengthened Fe-14Cr steels, Acta Mater. 127 (2017) 165–177, https://doi.org/10.1016/j.actamat.2017.01.026.
[50] K. Guan, L. Hua, Q. Wang, X. Zou, M. Song, Assessment of toughness in long term service CrMo low alloy steel by fracture toughness and small punch test, Nucl. Eng. Des. 241 (2011) 1407–1413, https://doi.org/10.1016/j.nucengdes.2011.01.031.
[51] I. Hilger, X. Boulnat, J. Hoffmann, C. Testani, F. Bergner, Y. De Carlan, F. Ferraro, A. Ulbricht, Fabrication and characterization of oxide dispersion strengthened (ODS) 14Cr steels consolidated by means of hot isostatic pressing, hot extrusion and spark plasma sintering, J. Nucl. Mater. 472 (2015) 206–214, https://doi.org/10.1016/j.jnucmat.2015.09.036.
[52] N. Sallez, C. Hatzoglou, F. Delabrouille, D. Sornin, L. Chaffron, M. Blat-Yrieix, B. Radiguet, P. Pareige, P. Donnadieu, Y. Bréchet, Precipitates and boundaries interaction in ferritic ODS steels, J. Nucl. Mater. 472 (2016) 118–126, https://doi.org/10.1016/j.jnucmat.2016.01.021.
[53] X. Boulnat, N. Sallez, M. Dadé, A. Borbély, J. Béchade, Y. De Carlan, J. Malaplate, Y. Brechet, F. de Geuser, A. Deschamps, P. Donnadieu, D. Fabregue, M. Perez, Influence of oxide volume fraction on abnormal growth of nanostructured ferritic steels during non-isothermal treatments: an in situ study, Acta Mater. 97 (2015) 124–130, https://doi.org/10.1016/j.actamat.2015.07.005.
[54] M. Dadé, J. Malaplate, J. Garnier, F. De Geuser, N. Lochet, A. Deschamps, Influence of consolidation methods on the recrystallization kinetics of a Fe-14Cr based ODS steel, J. Nucl. Mater. 472 (2016) 143–152, https://doi.org/10.1016/j.jnucmat.2016.01.019.